

# Computational Study of the Spectral Properties of Isospectrally Patterned Lattices

Peter Schmelcher<sup>1,2,\*</sup>

<sup>1</sup>*Zentrum für Optische Quantentechnologien, Fachbereich Physik,  
Universität Hamburg, Luruper Chaussee 149, 22761 Hamburg, Germany*

<sup>2</sup>*The Hamburg Centre for Ultrafast Imaging, Universität Hamburg,  
Luruper Chaussee 149, 22761 Hamburg, Germany*

(Dated: July 14, 2025)

We perform a computational spectral analysis of different isospectrally patterned lattices (IPL). Having been introduced very recently, the lattice Hamiltonian of IPL consist of coupled cells which possess all the same set of eigenvalues. The latter is achieved in a controllable manner by parametrizing the cells via the phases of the involved orthogonal (or unitary) transformations. This opens the doorway of systematically designing lattice Hamiltonians with unique properties by choosing correspondingly varying phases across the lattice. Here we focus on two-dimensional cells and explore symmetric as well as asymmetric IPL w.r.t. a given center. A tunable fraction of localized vs. delocalized eigenstates belonging to the three subdomains of the corresponding energy bands is demonstrated and analyzed with different measures of localization. In the asymmetric case the center of localization can be shifted arbitrarily by shifting the underlying phase grid. Introducing a complete phase revolution leads for low and high energies to two well-separated branches of localized states which finally merge with increasing energy into the branch of delocalized states. Remarkably, the localized states appear in near-degenerate pairs and this near-degeneracy is lifted upon entering the delocalization regime. A corresponding generalization to several phase revolutions is provided showing a characteristic nodal pattern among the near-degenerate eigenstates.

## I. INTRODUCTION

Symmetries play a pivotal role in physics. They code-terminate or even dictate the structure and form of interactions among the fundamental constituents of matter. Knowing the underlying symmetries the mathematical framework of group theory [1] provides us with a powerful toolbox which, in particular, allows us to predict physical properties without entering detailed, often expensive, numerical simulations. This statement holds across the disciplines of physics: in atomic physics [2] rotational symmetry classifies the eigenstates according to their angular momentum and imposes selection rules on their transitions whereas in solid state physics [3, 4] the spatial periodicity of crystals yields the Bloch theorem and conservation of the crystal momentum providing us with band structure theory. While the intimate connection between (discrete or continuous) symmetries and constants of motion holds for the above global symmetries, the situation is much less transparent and explored in the case of local symmetries, i.e. a symmetries that hold only for a subdomain of the overall space of a given physical system. Obviously, the possibilities of having local symmetries leads to more complex setups as compared to having corresponding global symmetries. Departing from e.g. crystals one well-known pathway to lower the symmetry is to replace the strict period-

icity by quasiperiodicity resulting in quasicrystals that exhibit a very special self-similar arrangement of local but no global symmetries. Their aperiodic long-range orders places them in the huge gap between crystalline and disordered phases [5–14]. Resultingly a rich behaviour emerges such as fractal energy spectra, critical localization of eigenstates, and eigenstates being arranged in so-called quasibands [15–19]. Specifically aperiodic one-dimensional sequences exhibit a local symmetry dynamics [14] that follows fundamental symmetry principles. However, local symmetries do not need to be arranged quasiperiodically, which is ultimately only a very special case, but can be distributed via emergence or design in a plethora of different ways. Fundamental for all of them is the fact that they show a generalization of the Bloch theorem where local symmetry-induced invariant non-local currents replace the quasimomentum [20]. These currents obey non-local continuity equations which have been established and exploited for both continuous [21] and discrete [22] setups and generalized to many-body interacting systems [23].

In a number of works based on the concept of local symmetries it has been demonstrated that their presence introduces novel properties into an otherwise unstructured system. Local symmetries can lead to sum rules for the invariant currents causing perfectly transmitting resonances for both quantum scattering [24] and electromagnetic wave propagation through multilayer [25] dielectric media. A computational framework for wave propagation that replaces the band structure calculation

---

\* peter.schmelcher@uni-hamburg.de

for crystals and addresses arbitrary combinations of local symmetries has been developed and applied [26]. The invariant currents have been detected experimentally and used to control the wave propagation in (lossy) acoustic waveguides [27] and in coupled photonic waveguide lattices [28]. Equipping a wave scattering device with more and more local symmetries it has been shown that the corresponding transport across this device is enhanced systematically [29].

A repeating observation in the analysis of locally symmetric devices is the fact that the localization of the underlying eigenstates tends to occur on subdomains with local symmetries. This has consistently been found in aperiodic long-range ordered setups [30] but even in setups which have only isolated local symmetries [29, 31] but are otherwise disordered. The origin of this localization behaviour was analyzed in depth [31] and is due to the fact that the eigenvalue spectrum of a subdomain of a lattice is invariant w.r.t. to symmetry transformations (reflection, translation). Therefore local symmetries imply (coupled) isospectral subdomains and the resulting degeneracies facilitate and allow to control the (de-)localization of the eigenstates as well as the splitting of the degenerate eigenvalues due to the couplings. These findings have recently lead [32] to the introduction of a new category of lattices: the isospectrally patterned lattices (IPL). The guiding construction principle behind IPL is the composite arrangement of isospectral (degenerate) cells that constitute an overall lattice. An immediate set of parameters that characterizes isospectral cells are the rotation angles of orthogonal transformations which create the cells on basis of an underlying orthogonally transformed diagonal matrix (see following section II). IPL can therefore be specified and designed according to the changes of the phases across the lattice.

A first recent exploration of IPL [32] has been focusing on finite (one-dimensional) lattices with a single phase varying according to a constant (discrete) gradient across the lattice. It has been demonstrated that the resulting 'band' structure of this inhomogeneous setup comprises three different regimes of localized versus delocalized states and crossovers between them. The localized states expand around a single center with increasing degree of excitation. The localization mechanism has been identified to emerge as a consequence of the competition between the phase gradient and the coupling among the isospectral cells and is therefore inherently different from other known localization mechanisms, such as Anderson localization [33]. The relative fraction of localized vs. delocalized states in each band can be controlled by changing the phase gradient.

Motivated by the above findings we perform in the present work an extensive computational study of IPL covering several setups with different phase profiles. This

includes asymmetrically placed phase profiles with no reflection symmetry and IPL with a single or several complete phase revolutions. We analyze their spectral properties in terms of eigenvalues and eigenstates, thereby addressing their band structure and localization properties. Specifically we discuss in section II our general setup, its relevant parameters and the appearance of the lattice Hamiltonian. To set the stage and be self-contained we provide in Section III a concise summary of the features of the previously investigated symmetric IPL. Section IV is then dedicated to a spectral analysis of the asymmetric IPL. Covering a complete phase revolution is the case of investigation in section V whereas several phase revolutions are addressed in section VI. Finally we conclude and provide perspectives of future research in section VI.

## II. SETUP AND HAMILTONIAN

Isospectrally patterned lattices consist of interconnected cells all of which share the same set of energy eigenvalues. To ensure the latter and provide a unique parametrization of the cells they are created by the orthogonal (or in general unitary) transformation  $\mathbf{O}_{\phi_m}$  of a given diagonal matrix  $\mathbf{D}$ , i.e. we have for the matrices describing the cells constituting the lattice the following appearance

$$\mathbf{A}_m = \mathbf{O}_{\phi_m}^{-1} \mathbf{D} \mathbf{O}_{\phi_m} \quad (1)$$

where  $m \in \{1, \dots, N\}$  stands for the cell index and  $\phi_m$  represents the set of phase angles  $\{\phi_m^1, \dots, \phi_m^{N_p}\}$ , or shortly phases, that characterizes and parametrizes the  $m$ -th cell. For cells of dimension  $K \times K$  there is  $N_p = \frac{K(K-1)}{2}$  such phases. These phases  $\phi_m$  can in principle be chosen arbitrarily but a properly designed IPL would, according to a first intuition, follow certain rules for the generation of the sequences of phases with varying sites of the lattice. The enormous flexibility in choosing these sequences adds to the richness of IPL. Finite lattices covering certain phase intervals for each of the  $\{\phi_m^1, \dots, \phi_m^{N_p}\}$  would be, pictorially speaking, inhomogeneous setups whereas periodic or quasiperiodic setups are possible by correspondingly choosing the phase difference between neighboring cells being rational or irrational and, principally, extending the lattice size to infinity. The previously found degeneracy-based (de-)localization mechanisms [31] in symmetry-related isospectral lattice domains provides a major additional motivation and raises expectations for novel spectral properties of the IPL. Our lattice Hamiltonian therefore consists of  $N$  cells and diagonal blocks  $\mathbf{A}_m, m \in \{1, \dots, N\}$  coupled via off-diagonal blocks  $\mathbf{C}_m, m \in \{1, \dots, N-1\}$  and takes on the following appearance

$$\mathcal{H} = \sum_{m=1}^N (|m\rangle \langle m| \otimes \mathbf{A}_m) + \sum_{m=1}^{N-1} (|m+1\rangle \langle m| \otimes \mathbf{C}_m + h.c.) \quad (2)$$

One might therefore take the viewpoint of considering the cell subspace as internal degrees of freedom and the cell index as external degree of freedom.  $N_s$  will in the following denote the total number of lattice sites within and across cells. In the previous first work on IPL [32] as well as here we will focus on the case  $K = 2$  resulting in a single phase parameter  $\phi$  which varies across the cells of the lattice. Consequently we have for a grid of a single phase  $\mathbf{A}_m = \mathbf{O}_{\phi_m}^{-1} \mathbf{D} \mathbf{O}_{\phi_m}$  or written out explicitly this yields

$$\begin{aligned} \mathbf{A}_m &= \begin{bmatrix} \cos \phi_m & \sin \phi_m \\ -\sin \phi_m & \cos \phi_m \end{bmatrix} \begin{bmatrix} d_1 & 0 \\ 0 & d_2 \end{bmatrix} \begin{bmatrix} \cos \phi_m & -\sin \phi_m \\ \sin \phi_m & \cos \phi_m \end{bmatrix} \\ &= \begin{bmatrix} d_1 \cos^2 \phi_m + d_2 \sin^2 \phi_m & (d_2 - d_1) \sin \phi_m \cos \phi_m \\ (d_2 - d_1) \sin \phi_m \cos \phi_m & d_1 \sin^2 \phi_m + d_2 \cos^2 \phi_m \end{bmatrix} \end{aligned} \quad (3)$$

Obviously  $\mathbf{A}_m$  possesses the determinant  $d_1 \cdot d_2$  and the trace  $d_1 + d_2$ . By substituting  $\phi_m = \psi_m + \frac{\pi}{4}$  into the above expression one obtains

$$\mathbf{A}_m = \frac{d_1 + d_2}{2} \mathbb{1} + \frac{d_2 - d_1}{2} \begin{bmatrix} \sin(2\psi_m) & \cos(2\psi_m) \\ \cos(2\psi_m) & -\sin(2\psi_m) \end{bmatrix} \quad (4)$$

which splits  $\mathbf{A}_m$  into a part proportional to the identity matrix, i.e. a global offset, and a traceless contribution comprising its nontrivial part. The coupling between the cells will be chosen as  $\mathbf{C} = \mathbf{C}_m = \frac{\epsilon}{2} (\sigma_x + i\sigma_y)$  and we use open boundary conditions for our lattice. Here  $\epsilon$  denotes the coupling strength and  $\sigma_i, i = x, y$  are the corresponding  $2 \times 2$  hermitian and unitary Pauli matrices. Note that the above-designed lattices represent one-dimensional configurations/chains but could easily be generalized to higher dimensions by introducing the corresponding off-diagonal couplings. The broad class of IPL contains several important special models. The SSH-model (see ref.[34] and references therein) is obtained by making all phases across the lattice of equal value  $\psi = \frac{\pi}{2}$  such that, after subtracting the global offset value, the diagonal entries vanish. The dimerized character stems then from the intracell coupling and the intercell coupling (see below). The (time-independent) Rice-Mele model is obtained for a constant but arbitrary phase  $\psi$  (see [35] and references therein). We will focus in the present work on finite lattices covering a finite interval of the phase  $\phi$  and possessing a constant phase difference between neighboring cells.

### III. SYMMETRIC IPL

To set the stage for a prototype IPL and in order to be self-contained let us firstly recapitulate and expand on the spectral properties of what we call a symmetric IPL which has been explored previously [32]. For the single phase  $\phi_m$  we choose an equidistant grid of phase values centered around the specific value  $\frac{\pi}{4}$ . The motivation herefore lies in the previous observation [31] that isospectrally related cells that gradually change across the lattice might offer the possibility to steer the localization properties of the lattice eigenstates. The phase range covered by the lattice is then given by  $[\frac{\pi}{4} - \frac{L}{2}, \frac{\pi}{4} + \frac{L}{2}]$  with  $L = \frac{\pi}{4} \cdot \frac{1}{L_f}$  where  $L_f$  is a scaling factor for the phase interval covered by the lattice. For the individual phase value of the  $m$ -th cell we have  $\phi_m = \frac{\pi}{4} - \frac{L}{2} + \frac{m-1}{N-1}L$ ,  $m \in \{1, \dots, N\}$ . The specific center value  $\phi = \frac{\pi}{4}$  is chosen because for this phase the corresponding cell eigenvectors read  $(\cos \phi, -\sin \phi)$  with the eigenvalue  $d_1$  and  $(\sin \phi, \cos \phi)$  with the eigenvalue  $d_2$  which are the diagonal entries of the matrix  $\mathbf{D}$ . Obviously, these are for  $\phi = \frac{\pi}{4}$  'maximally delocalized' whereas  $\phi = 0, \frac{\pi}{2}$  renders one of the two components of the eigenvectors zero. Additionally, our lattice shows, by choosing for the center cell  $\phi = \frac{\pi}{4}$ , an inversion symmetry.

A note is in order concerning our use of the term (de-)localized (eigen-)states. Since we address in this work exclusively finite lattices we apply the term localized eigenstates to those states which possess a substantial amplitude solely inside the lattice and dont reach the boundaries of the lattice or which reach only one edge of the lattice. Delocalized eigenstates extend over the complete lattice. As we shall see localized and delocalized states are not intermingled but occur in specific energetical regimes and are separated by a finite system localization delocalization crossover (FLDC).

Let us start our analysis by inspecting the energy eigenvalue spectrum for an IPL for an equidistant  $\phi$  lattice with  $\frac{\pi}{8} \leq \phi \leq \frac{3\pi}{8}$ , for  $d_2 = 2, d_1 = 2, L_f = 1.0, \epsilon = 0.2, N_s = 1002$ , see Fig.1. Fig.1(a) shows the eigenvalues which are arranged in two bands separated by a large gap. The individual bands show a behaviour which is distinctly different from the cosine-like dispersion relation for a monomer tight-binding chain: one observes three different energetical subdomains for each band, labeled by A,B,C for the energetically lower band in Fig.1, for which the slopes are different. They indicate a qualitatively different behaviour of the level structure for these different subdomains. This becomes more pronounced when inspecting the energy eigenvalue spacing instead of the absolute eigenvalues, as can be seen in Fig.1(b). The energy spacing with increasing degree of excitation shows a very different behaviour in the three subdomains

A,B,C. In subdomain A the spacing is slightly decreasing with increasing

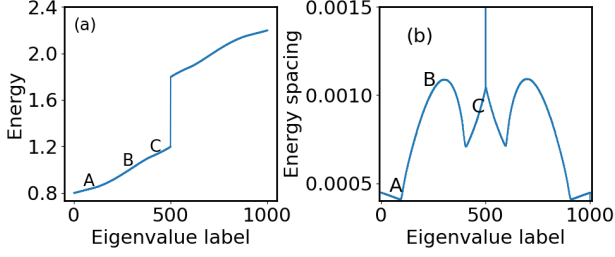


Figure 1. (a) Energy eigenvalue spectrum of the equidistant  $\phi$  lattice with  $\frac{\pi}{8} \leq \phi \leq \frac{3\pi}{8}$ , for  $d_1 = 1, d_2 = 2, L_f = 1.0, \epsilon = 0.2, N_s = 1002$ . The vertical line indicates the energy gap between the two bands. (b) The corresponding energy eigenvalue spacing with increasing degree of excitation. Each band consists of three different domains labeled by A, B and C for the lowest band. The energy level spacing shows a much more abrupt transition between those domains as compared to the energy eigenvalue spectrum itself.

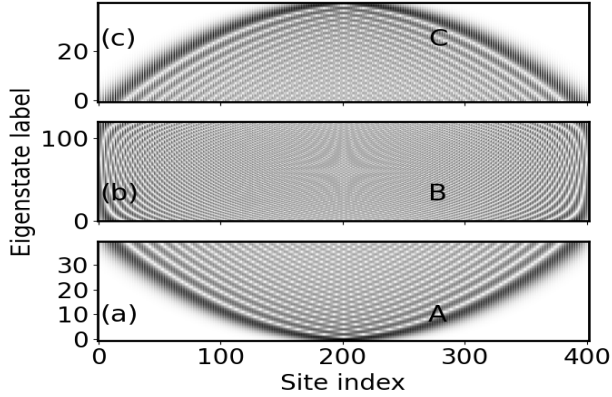


Figure 2. Grey scale eigenstate map showing the absolute values of all eigenstate components for the lower band of the spectrum of the equidistant  $\phi$  lattice with  $\frac{\pi}{8} \leq \phi \leq \frac{3\pi}{8}$ , i.e. placed symmetrically w.r.t.  $\frac{\pi}{4}$ , for  $d_1 = 1, d_2 = 2, L_f = 1.0, \epsilon = 0.2, N_s = 402$ . The grey scale has been renormalized for each eigenstate row. The labeling of the eigenstates (vertical axis) is reset to zero within each energy domain with a total of 201 states. (a,b,c) show the eigenstate profiles according to the three energy domains A,B,C of the lower band in Fig. 1; domains A and C show centered and localized eigenstates whereas domain B consists of eigenstates that extend over the complete lattice and reach out to its boundaries.

degree of excitation but is in zeroth order approximation constant. In subdomain B the spacing behaves highly nonlinear: it first increases in an approximately parabolic manner and then, after reaching a maximum, it decreases correspondingly ending at a point which is at a higher energy compared to the beginning of the subdomain B. Finally in regime C the energy spacing increases strongly in a slightly nonlinear way, meaning that a linear fit represent a moderately good approximation in this regime. This behaviour repeats in an inverted fashion in the second band.

The question which arises in view of the characteristic eigenvalue spectrum shown in Fig.1 addresses the origin of the observed spectral behaviour. To illuminate this we show in Fig.2 a grey scale eigenstate map presenting the absolute values of all eigenstate components for all eigenstates of the lower band of the spectrum for an equidistant  $\phi$  lattice with  $\frac{\pi}{8} \leq \phi \leq \frac{3\pi}{8}$  for the same parameters as in Fig.1 except for the value  $N_s = 402$ . This map is partitioned according to the subdomains A,B,C of Fig.1 in the subfigures Fig.2(a,b,c). We observe that regions A and C correspond to localized eigenstates which are centered around the center cell with  $\phi = \frac{\pi}{4}$ . While the global ground state shows an envelope behaviour of approximately Gaussian character [31] we observe (not shown here) with increasing degree of excitation an increasing number of nodes of this envelope. The localization mechanism [31] involves the competition between the phase gradient across the lattice and the coupling among the cells. Emerging from the center cell the localized eigenstates spread with increasing degree of excitation until they reach the boundary of the lattice for the eigenstate at the crossover from subdomain A to B or from subdomain B to C in the reverse manner. In contrast to this subdomain B consists of delocalized eigenstates that extend over the complete lattice and reach to its boundaries.

To quantify the above localization behaviour of the eigenstates of the IPL we determine their inverse participation ratio which is defined as  $r = \sum_{i=1}^N |\psi_i|^4 \in [N^{-1}, 1]$ , where  $\psi_i$  is the eigenvector component on site  $i$  of a given eigenstate  $\psi$ . The IPR of an eigenstate possesses the maximal value one for an eigenstate localized on a single site of the lattice and it has the minimal value  $\frac{1}{N}$  for a state uniformly extended over the lattice. Fig.3 shows the IPR for all eigenstates of the lowest band shown in Fig.2. Starting from the ground state we observe a decrease of the IPR with increasing degree of excitation in the subdomain A until the crossover to subdomain B takes place and within the latter a plateau-like behaviour of the IPR occurs. Finally, in subdomain C, the IPR raises again with further increasing degree of excitation, reflecting the increasing degree of localization culminating again at the upper band edge into a Gaussian-like envelope be-

haviour of the corresponding eigenstate. Therefore, the IPR clearly signals the two FLDC occurring in each band.

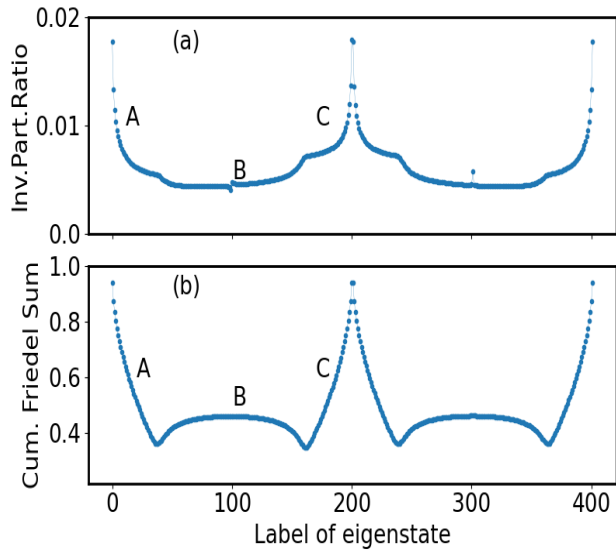


Figure 3. (a) The inverse participation ratio for all eigenstates across both bands. Parameters are the same as in Fig. 2. (b) The corresponding cumulative Friedel sum. Both measures for localization reflect the domains A,B,C: eigenstates in A,C possess typically higher values and rapidly change with varying degree of excitation for both the inverse participation ratio and the cumulative Friedel sum whereas eigenstates in B form (apart from the corresponding transition region) a flat valley of low values.

The IPR as a localization measure does not depend on the position at which a state is localized within a given lattice system. It is, however, largely insensitive to the spatial state profiles [36]. To address this issue, and exploit an alternative localization measure, we employ the cumulative Friedel sum (CFS) of a given state [29]. The CFS is based on a measure developed in [36] which is inspired by the Friedel sum rule [37]. It reflects more details of the spatial profile by using its cumulative sum  $P_n = \sum_{m=1}^n |\psi_m|^2$  up to site  $n$  and reads

$$f = \frac{1}{2N} \left| \sum_{n=1}^N (e^{2\pi i P_n} + 1) \right| \in [N^{-1}, 1] \quad (5)$$

Larger (smaller) values for the CFS indicates a more (less) localized state, though now taking into account its total spatial extent instead of only its site participation. Inspecting the CFS for the eigenstates in Fig.3(b) a similar behaviour to that of the IPR can be observed: in

the subdomain A, starting with the ground state in the band, we have a strong decrease of the CFS values. In subdomain B there is a minor variation of the CFS values whereas in subdomain C a strong increase is obtained for an increasing degree of excitation. All of this behaviour reflects again the fact that the eigenstates in the subdomains A,C correspond to localized states that gradually delocalize and vice versa, and that the eigenstates in subdomain B are all delocalized. It should be noted that the absolute values of the CFS as well as their variations are much larger compared to those of the IPR.

Let us now inspect how the above-observed behaviour of a divided eigenstate space consisting of localized and delocalized states changes if we change the relevant parameters. For the above-considered case we had a parameter value  $L_f = 1.0$  corresponding to a total phase interval  $\frac{\pi}{8} \leq \phi \leq \frac{3\pi}{8}$ . Let us now focus on the case  $L_f = 0.5$  for which  $0 \leq \phi \leq \frac{\pi}{4}$ . Fig.4 shows the eigenstate map for this parameter value, which demonstrates that almost all states are localized and subdomains A and B have taken over the eigenstate profile map where subdomain C consists only of a very few 'limiting' states. This is indicative of the fact that, with varying parameter  $L_f$ , and consequently with varying phase gradient the fraction of localized versus delocalized eigenstates can be varied arbitrarily. Indeed, the inset of Fig.4 shows that this fraction can be tuned continuously from the value zero to one while varying  $L_f$  from 0.5 to very large values. It should be noted that for  $L_f \rightarrow \infty$  our IPL becomes periodic since the phase interval 'collapses' to a single value and in this case only extended states survive.

It is instructive to compare the above results on the eigenstate localization properties with examples of random distributions. To this end Fig.5(a) shows the eigenstate map for a lattice with a random sequence of on-site energies for the values one and two, but otherwise the same parameter values as in Fig.2 except for  $N_s = 302$ . There are two obvious major differences of the localization behaviour of the eigenstates compared to our IPL (see Fig.2). First, the eigenstates do not possess a single center as it is the case for the IPL, but are, as expected, localized around many different centers reflecting the random design with many 'impurities'. Second, the localization length of those eigenstate profiles is much smaller compared to the deterministic localization length of the IPL eigenstates which is a 'cooperative' effect of the phase gradient and the coupling strength. To quantify the localization behaviour Fig.5(b) shows the corresponding IPR which exhibits irregular fluctuations on a scale much larger than the typical values occurring for the IPL (see Fig.3). This is, as mentioned-above, due to the stronger localization in the random case. While the IPR for the IPL varies smoothly with increasing degree of excitation, the IPR of our random on-site energy case



shows no such smooth behaviour.

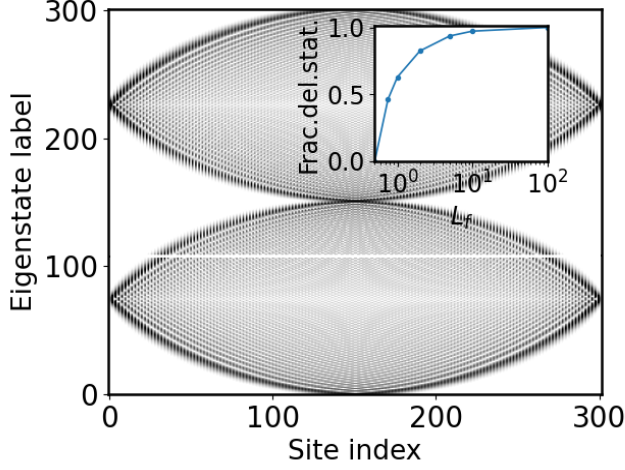


Figure 4. Grey scale eigenstate map showing the absolute values of all eigenstate components for the equidistant  $\phi$  lattice with  $0 \leq \phi \leq \frac{\pi}{2}$ , i.e. placed symmetrically w.r.t.  $\frac{\pi}{4}$ , for  $d_1 = 1, d_2 = 2, L_f = 0.5, \epsilon = 0.3, N_s = 302$ . Almost all eigenstates are localized in this case. The inset shows the fraction of delocalized states with varying parameter  $L_f$  which relates to the corresponding phase gradient. Here  $N_s = 1002, \epsilon = 0.2$ . This demonstrates that the fraction of (de-)localized states can be varied from no extended states to extended states only.

As a second case of comparison we show in Fig.6(a) the eigenstate map for an IPL with randomly chosen phases in the range  $\frac{\pi}{8} \leq \phi \leq \frac{3\pi}{8}$ . Also here we observe that there is no smooth structures and crossover between localized and delocalized states as for the symmetric IPL discussed above. The band(s) consist exclusively of differently centered localized eigenstates. However, a comparison with Fig.5(a) reveals that the localization length is typically larger compared to the random on-site energy case. Indeed, Fig.6(b) shows that the irregularly fluctuating values of the IPR are consistently lower for the case of phase randomization, but still significantly larger compared to our original symmetric IPL (see Fig.3(a)).

Finally, a note is in order concerning the impact of the (de-)localized state decomposition of the IPL upon contacting it from the outside, i.e. probing the IPL transport properties. It is to be expected that for the energetical subdomains A,C of localized eigenstates the transport would be strongly suppressed whereas for the delocalized eigenstate subdomain B transport takes place. Therefore, the IPL would allow us to controllably provide transport in an energetical window determined by the width of the subdomain of delocalized states, which is tunable. A detailed investigation of the transport proper-

ties of IPL goes however beyond the scope of the present investigation which focuses on its spectral properties.

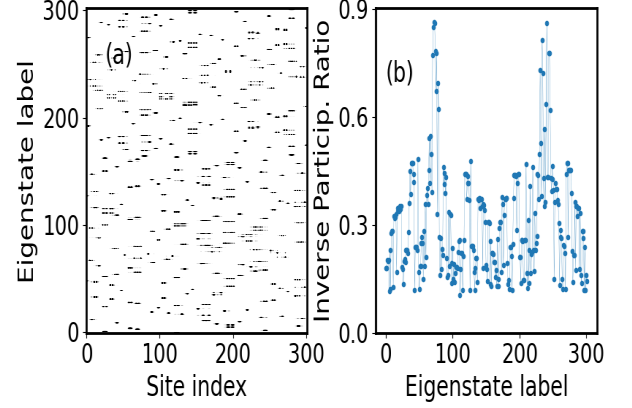


Figure 5. (a) Grey scale eigenstate map showing the absolute values of all eigenstate components for a lattice with randomly chosen on-site energies  $d_1 = 1, d_2 = 2$  and a coupling strength  $\epsilon = 0.2$  for  $N_s = 302$ . Inspection by eye shows already that the spreading of the eigenstates is overall by orders of magnitude smaller than the lattice size. (b) The corresponding inverse participation ratio for all eigenstates is irregularly oscillating opposite to the smooth behaviour observed for the isospectrally patterned lattice, see Fig.3. It is by orders of magnitude larger due to the strong localization.

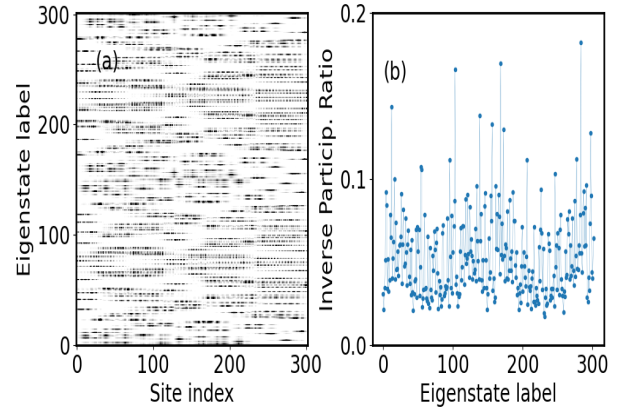


Figure 6. (a) Grey scale eigenstate map showing the absolute values of all eigenstate components for a lattice with randomly chosen phases in the range  $\frac{\pi}{8} \leq \phi \leq \frac{3\pi}{8}$  and  $d_1 = 1, d_2 = 2$  with a coupling strength  $\epsilon = 0.2$  for  $N_s = 302$ . (b) The corresponding inverse participation ratio for all eigenstates. For this phase disorder case, the eigenstates are much more spreading out as compared to the random on-site energy case, see Fig.5, also reflected in the shown smaller values of the inverse participation ratio.

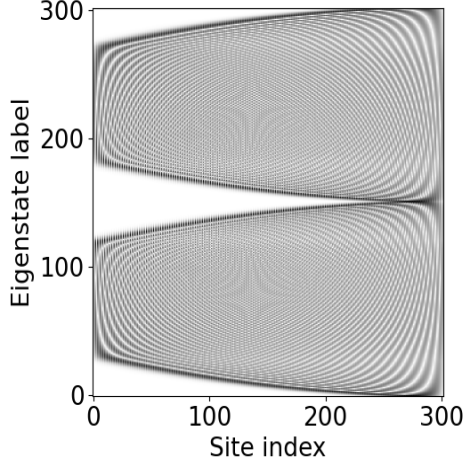


Figure 7. Grey scale eigenstate map showing the absolute values of all eigenstate components for both bands of the spectrum of the equidistant  $\phi$  lattice with  $\frac{\pi}{8} \leq \phi \leq \frac{\pi}{4}$ , i.e. placed asymmetrically w.r.t.  $\frac{\pi}{4}$ , for  $d_1 = 1, d_2 = 2, L_f = 2.0, \epsilon = 0.3, N_s = 302$ . The grey scale has been renormalized for each eigenstate row. Eigenstates are now centered around the right edge of the lattice and gradually extending towards the left edge with increasing (decreasing) degree of excitation from the lower (upper) band edge. In between is a regime of delocalized states extending over the complete lattice.

#### IV. ASYMMETRIC IPL

There is many different possibilities for choosing the sequence of phases underlying an IPL. In the previous section we have chosen an equidistant phase grid covering a finite total phase interval  $[\frac{\pi}{4}(1 - \frac{1}{2L_f}), \frac{\pi}{4}(1 + \frac{1}{2L_f})]$  where the phase distribution is placed symmetrically around its center value  $\phi = \frac{\pi}{4}$ . As a natural first extension of this symmetric IPL we will now break this inversion symmetry and place the phase interval covered by the lattice asymmetrically around the value  $\frac{\pi}{4}$ .

Fig.7 shows the eigenstate map for the completely asymmetric case with  $\frac{\pi}{8} \leq \phi \leq \frac{\pi}{4}$  where  $\frac{\pi}{4}$  occurs at the edge of the lattice. We observe that the ground state is now localized at the right edge of the lattice and, with increasing degree of excitation, the eigenstates extend increasingly into the interior of the lattice, thereby always reaching out to the right edge of the lattice. This constitutes the first subdomain of each band. The second subdomain consists of delocalized states extending over the complete lattice whereas the third subdomain possesses the reverse structure of the first one. We therefore encounter, similar to the symmetric IPL, also two FLDC for the asymmetric IPL. Choosing the phase interval in between the

symmetric and completely asymmetric case (not shown here) will shift the location/centering of the ground state and consequently of all following excited localized states of the corresponding first subdomain continuously from the center of the lattice to its edge. This tunability exists equally for the case of a left edge-based localized eigenstate domain simply by choosing for the completely asymmetric case the phase interval  $\frac{\pi}{4} \leq \phi \leq \frac{3\pi}{8}$ . In a nutshell, breaking the inversion symmetry w.r.t.  $\frac{\pi}{4}$  of the covered phase interval of the lattice allows to continuously shift the centering of the localized eigenstate subdomains thereby leading to a tunable asymmetry.

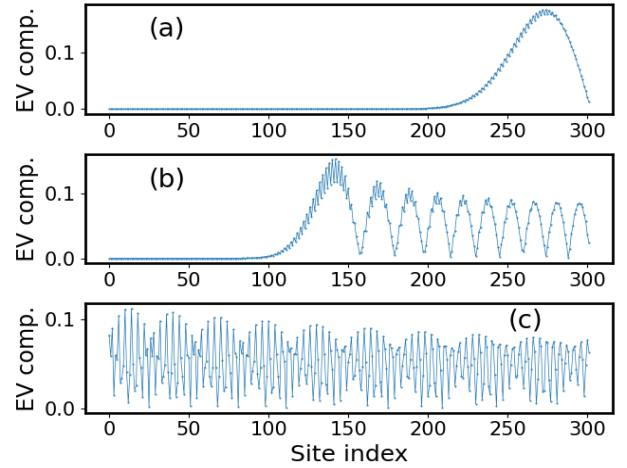


Figure 8. Individual eigenstate profiles (magnitude of the eigenvector components) for the ground state, the 10th and 70th eigenstate in subfigures (a,b,c), respectively. Equidistant  $\phi$  lattice with  $\frac{\pi}{8} \leq \phi \leq \frac{\pi}{4}$ , i.e. placed asymmetrically w.r.t.  $\frac{\pi}{4}$ , for  $d_1 = 1, d_2 = 2, L_f = 2.0, \epsilon = 0.3, N_s = 302$ . The asymmetric oscillatory structure extending over (parts of) the lattice is clearly visible.

Fig.8 shows the eigenstate profiles for the ground state, the 10th and 70th eigenstate in subfigures (a,b,c), respectively, for the equidistant  $\phi$  lattice with  $\frac{\pi}{8} \leq \phi \leq \frac{\pi}{4}$ , corresponding to Fig.7. The ground state in Fig.8(a) is, as discussed above, localized next to the right boundary of the lattice and possesses an asymmetric profile around its maximum with a tail reaching into the inner part of the lattice. The 10th eigenstate (see Fig.8(b)) shows a strongly regularly oscillating behaviour emerging from the right edge of the lattice and covering slightly more than half of the lattice size. This state, obviously, still belongs to the subdomain of localized states near the lower band edge. Finally Fig.8(c) shows the 70th eigenstate which exhibits high frequency oscillations and some beating behaviour with a significantly lower frequency: it

extends over the complete lattice and therefore belongs to the subdomain of delocalized states.

Let us contemplate about the impact of the asymmetric localized states particularly in the above-shown case of complete asymmetry. If we contact this asymmetric IPL via left and right suitably matched leads it can be conjectured that the above-discussed right centered localized states (subdomain A) would allow for a penetration of the eigenstates (of the IPL plus leads) that emerge from the right into the IPL with some tunable and energy-dependent depth. For the same energies in the subdomain of localized states, a penetration from the left lead would be strongly suppressed. For higher energies (subdomain B) transport across the IPL would take place and would be followed (subdomain C) by an inverted scenario as compared to subdomain A.

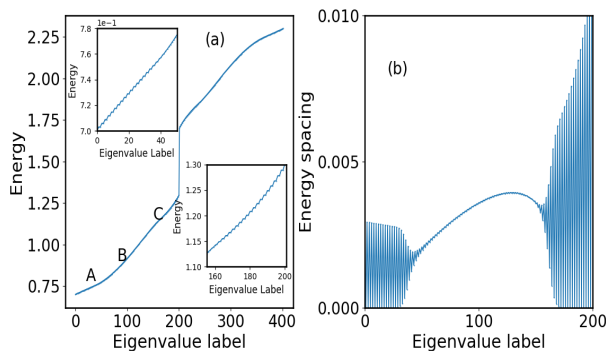


Figure 9. (a) Energy eigenvalue spectrum of the equidistant  $\phi$  lattice with one complete oscillation within the interval  $\frac{\pi}{8} \leq \phi \leq \frac{3\pi}{8}$ , for  $d_1 = 1, d_2 = 2, L_f = 1.0, \epsilon = 0.3, N_s = 402$ . A, B and C indicate the different domains in the corresponding bands. The insets show corresponding magnifications for the regimes at the lower (upper inset) and upper (lower inset) band edge of the lower band showing a plateau-like structure. (b) The energy eigenvalue spacing spectrum for the first band. The latter shows that the energy levels are for low (high) energies in the band approximately pairwise degenerate whereas in the central part of the band this (approximate) degeneracy is lifted.

## V. IPL WITH A SINGLE PHASE REVOLUTION

Let us now explore the case for which the phase variation across the finite lattice is such that it increases first and decreases thereafter. We therefore consider an oscillation of the phase covering a phase interval  $\frac{\pi}{8} \leq \phi \leq \frac{3\pi}{8}$  first by increasing the phase and, upon reaching the turning point  $\frac{3\pi}{8}$ , by decreasing the phase with a constant phase difference from cell to cell. Such an oscillatory behaviour includes within each half oscillation the point of inver-

sion symmetry  $\frac{\pi}{4}$  for the symmetric IPL. Fig.9(a) shows the energy eigenvalue spectrum with increasing degree of excitation. Also in this case three different distinct subdomains can be identified for each band. A magnification of the regions around the lower (upper inset) and upper (lower inset) band edge are shown as insets. Here a plateau-like structure can be observed which is more pronounced the closer we are energetically to the corresponding band edge. This structure dissolves as we move closer in energy towards the center of the band. Upon inspection of the energy eigenvalue spacing, see Fig.9(b), we observe a near zero value for every second spacing: the energy eigenvalues arrange in near degenerate pairs, being closer to degeneracy the closer the energy is to the band edge. It is important to note that the ground state is non-degenerate (hardly visible in Fig.9(a,b) due to the finite resolution) and the pairing starts only with the excited states.

Moving with the energy towards the center of the band the near degeneracies are lifted beyond the  $\approx 40$ -th eigenstate (see Fig.9(b)) and the energy spacing exhibits an arc-like behaviour of non-degenerate eigenvalues. The latter structure occupies a large central part of the spectrum. It is important to note that the extension of the subdomains A,B,C of localized vs. delocalized states does not coincide with the regimes for which near degenerate pairs occur or not: near degeneracy is encountered only for localized states sufficiently far from the boundaries of the IPL. A few remarks are in order and are illuminating w.r.t. the observed spectral features: let us address some simplified models which are more or less different from the IPL but possess all the property that they are lattices of coupled isospectral cells with a single complete phase revolution. Our first simplified model goes as follows. Taking as a first half the IPL for e.g.  $\frac{\pi}{8} \leq \phi \leq \frac{3\pi}{8}$  and augmenting this lattice by a decoupled second half lattice which is the inverted of the first one, it goes without saying that we will obtain a spectrum exclusively consisting of (exactly) doubly degenerate pairs of eigenvalues, due to the isospectrality of the (decoupled) two halves of the lattice. It should be noted that our IPL for a single complete phase revolution is not inversion symmetric around  $\frac{3\pi}{8}$  due to the 'non-inverted' phase-based cells in the course of the construction of the IPL. For our second model we use the first model and introduce a coupling between the two halves of it. We then observe the formation of near degenerate pairs close to the band edges as described above for the IPL. This two-fold near degeneracy holds also for the ground state, opposite to what we have observed above for the IPL. Further differences between this second model and the IPL reveal themselves only upon inspecting the eigenstate profiles, which we will accomplish as a next step.

Fig.10(a) shows the eigenstate map for the IPL for both



bands of the spectrum for an equidistant  $\phi$  lattice with one complete oscillation within the interval  $\frac{\pi}{8} \leq \phi \leq \frac{3\pi}{8}$ . Now two centered series of localized states are observed, each emerging and spreading around the symmetry point  $\phi = \frac{\pi}{4}$  which is met twice in the course of a single phase revolution. Upon increasing the energy these localized states meet the boundaries of the IPL where an FLDC is encountered. As a consequence, with further increasing energy, a subdomain of states delocalized across the complete IPL occurs. Following on this subdomain localization takes over again culminating in a state at the upper band edge of the lower band which consists again of two well-isolated centered distributions around  $\phi = \frac{\pi}{4}$ . This behaviour repeats for the upper band.

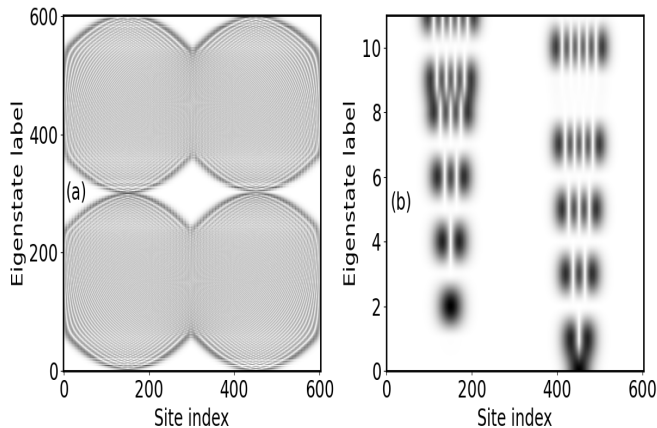


Figure 10. (a) Grey scale eigenstate map showing the absolute values of all eigenstate components for both bands of the spectrum of the equidistant  $\phi$  lattice with one complete oscillation within the interval  $\frac{\pi}{8} \leq \phi \leq \frac{3\pi}{8}$  for  $d_1 = 1, d_2 = 2, \epsilon = 0.3, N_s = 602$ . The grey scale has been renormalized for each eigenstate row. We observe two centers from which localized eigenstates spread (lower band edge) with the reverse process, i.e. focusing, happening at the upper band edge. (b) Magnification of the grey scale eigenstate map for the twelve energetically lowest eigenstates. The nodeless localized states appear spatially isolated at different energies in the first and second half of the (finite) lattice. Near degenerate and spatially separated eigenstates (such as the states with eigenvalue label one and two) belonging to the first and second half of the lattice possess a different nodal structure.

Fig.10(b) allows for a closer inspection of the profiles of the energetically lowest states. As we know from Fig.9(a,b) we have energetically near degenerate pairs of eigenstates in the low energy and high energy part of the spectrum and a ground state which is non-degenerate. Surprisingly Fig.10(b) now shows that these near degen-

erate pairs consist of well-localized eigenstates each centered around  $\phi = \frac{\pi}{4}$  in the first/second half of the oscillation of the phase, and, importantly, with a different nodal structure i.e. they belong to a different neighboring degree of excitation. This is to be contrasted with the features of the second simplified model (coupled inversion symmetric setup) addressed above showing a near degenerate pairing of localized eigenstates including the ground state and in particular showing for the eigenstates of a given pair the same degree of excitation i.e. nodal structure.

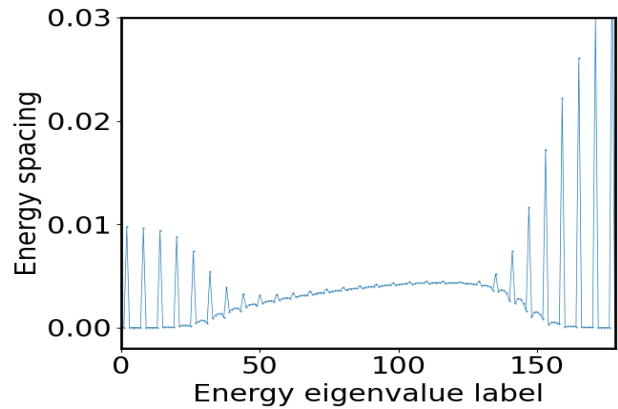


Figure 11. Energy eigenvalue spacing spectrum of the equidistant  $\phi$  lattice with three complete oscillations within the interval  $\frac{\pi}{8} \leq \phi \leq \frac{3\pi}{8}$ , for  $d_1 = 1, d_2 = 2, L_f = 1.0, \epsilon = 0.3, N_s = 362$ . A six-fold near degeneracy is observed for energies close to the lower (upper) band edge which is lifted in the center of the band.

## VI. IPL WITH SEVERAL PHASE REVOLUTIONS

Finally we focus on an IPL with several phase oscillations taking place in the interval  $\frac{\pi}{8} \leq \phi \leq \frac{3\pi}{8}$ . Fig.11 shows the eigenvalue spacing spectrum with increasing degree of excitation for the case of three complete oscillations and the total number of sites being  $N_s = 362$  for the energetically lower band. The isolated peaks between multiple near zero spacing values indicate that there exist multiplets of near degenerate eigenstates separated by 'gaps'. Indeed, a closer inspection reveals that the ground state is three-fold near degenerate whereas all excited states are six-fold near degenerate. This statement holds for energies in the low energy domain whereas beyond the  $\approx 50$ -th eigenstate this near degenerate character is lost and the center of the band is constituted by energetically well-separated eigenstates, similarly to what has been observed in section V for an IPL with a single oscillation.

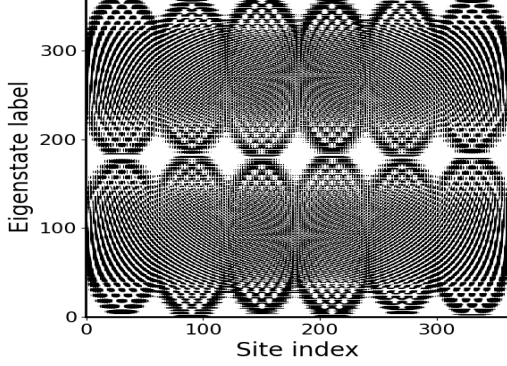


Figure 12. Grey scale eigenstate map showing the absolute values of all eigenstate components for both bands of the spectrum of the equidistant  $\phi$  lattice with three complete oscillations within the interval  $\frac{\pi}{8} \leq \phi \leq \frac{3\pi}{8}$  for  $d_1 = 1, d_2 = 2, \epsilon = 0.3, N_s = 362$ . The vertically displaced sequences of eigenstate profiles for the localized eigenstates in the first and second halves of the lattice oscillations is visible upon close inspection.

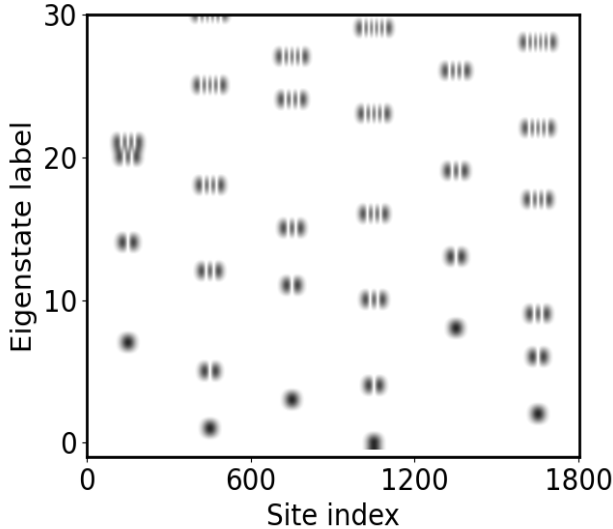


Figure 13. Grey scale eigenstate map showing the absolute values of all eigenstate components for energy eigenstates close to the lower bands band edge for the equidistant  $\phi$  lattice with three complete oscillations within the interval  $\frac{\pi}{8} \leq \phi \leq \frac{3\pi}{8}$ . Parameters are  $d_1 = 1, d_2 = 2, \epsilon = 0.3, N_s = 1802$ .

Finally, approaching the upper band edge the reverse process of near degenerate multiplet formation is observed. The energy spacing between the near degenerate multi-

plets is much larger and varies more strongly with increasing degree of excitation for the eigenstates close to the upper band edge as compared to those close to the lower band edge.

Fig.12 shows the corresponding eigenstate map which, as expected, shows subdomains of localized and delocalized eigenstates in each band. Now, however, we have a six-fold centering of the well-separated eigenstates in the subdomain of localized eigenstates and an increasing spreading of them with increasing degree of excitation finally culminating in the corresponding FLDC. Three near-degenerate states including the (global) ground state can be identified. This becomes even more transparent and evident upon inspecting Fig.13 which shows the eigenstate map for the low energy part of the first band. Here also the different degree of excitation and nodal structure occurring pairwise in the six-fold near degenerate multiplets can be observed. For reasons of illustration we have here chosen  $N_s = 1802$ .

## VII. CONCLUSIONS AND OUTLOOK

Isospectrally patterned lattices are composed of cells with the same spectral content i.e. possessing the same eigenvalue spectrum. This spectral degeneracy of the isolated cells is a key ingredient in order to steer the localization properties of the lattice eigenstates once a coupling between the cells in the lattice is turned on. What makes the IPL easily accessible and straightforward to design is their parametrization via the phases/angles. Different cells of the same spectral content are connected via an orthogonal or unitary transformation for a given set of transformation angles. The overall lattice can then be systematically designed in many different ways: there is many possible choices of the variation of the angles across the lattice. In a first work [32] the focus was on an equidistant phase lattice covering a finite interval centered around an inversion center  $\frac{\pi}{4}$ . The resulting 'band' structure consists two bands each comprising three different regimes of localized and delocalized states for the inherently finite lattice. The localization mechanism is based on a competition of the phase gradient and the coupling among the cells and leads to a single center localization behaviour with a characteristic length scale and a systematic increased spreading around this center with an increasing degree of excitation. Varying the phase gradient allows for a tuning of the fraction of localized versus delocalized states from only localized to exclusively delocalized states.

In the present computational study of the IPL we have detailed their properties and have, in particular, explored the spectral properties of several novel setups. Among these is, in the first instance, an equidistant phase lat-

tice which is centered asymmetrically around the distinct value  $\frac{\pi}{4}$ . We observe that the eigenstates are now also de-centered and can be shifted continuously from the center of the lattice to its edges. Left and right localization of the eigenstates allow for a controllable depth of 'penetration' of them into the interior of the lattice. In a second step we investigated a phase lattice with a complete revolution of the phase. This setup leads to some peculiar spectral structures. While the three subdomains of each band still persist their spectral content has changed substantially. Importantly, now the single center localization of the eigenstates is replaced by a two center localization behaviour. Close to the band edges a pairwise near degeneracy is encountered which lifts with increasing degree of excitation of the localized eigenstates and finally disappears completely in the regime of delocalized eigenstates. The reverse process is found close to the upper band edge. Notably the ground state is non-degenerate in this scenario and the near degenerate pairs involve localized eigenstates with a different nodal structure. This generalizes to the case of several phase revolutions which has also been analyzed in the present work.

There is several open directions of investigation for the

IPL in the future. One of them is based on the observation that with increasing coupling among the cells the band gap closes and opens again - here the questions is whether this is indeed accompanied by a topologically nontrivial behaviour for our finite inhomogeneous (non-periodic !) IPL setup and what the topological markers would be. Another direction would be to extend the current finite lattices to, principally, infinite ones and let the phase, according to some 'rule', evolve indefinitely. Both periodic and non-periodic cases are then possible. These are only two out of several possible future routes of investigation of IPL.

## VIII. ACKNOWLEDGMENTS

The author acknowledges many inspiring discussions with F.K. Diakonov. This work has been supported by the Cluster of Excellence 'Advanced Imaging of Matter' of the Deutsche Forschungsgemeinschaft (DFG) - EXC 2056 - project ID 390715994.

- 
- [1] M. Hamermesh, Group Theory and Its Applications to Physical Problems, Dover Books on Physics and Chemistry, 1989.
  - [2] H. Friedrich, Theoretical Atomic Physics, Springer Berlin Heidelberg, 2010.
  - [3] N.W. Ashcroft and N.D. Mermin, Solid State Physics, Holt-Saunders, 1976.
  - [4] J. Singleton, Band Theory and Electronic Properties of Solids, Oxford Master Series in Condensed Matter Physics, Oxford University Press 2001.
  - [5] E. Maciá Barber, Aperiodic Structures in Condensed Matter, Fundamentals and Applications, Series in Condensed Matter Physics, CRC Press 2009.
  - [6] E. Maciá-Barber, Quasicrystals, Fundamentals and Applications, CRC Press 2021.
  - [7] D. Shechtman, I. Blech, D. Gratias, and J. W. Cahn, Metallic phase with long-range orientational order and no translational symmetry, Phys.Rev.Lett. 53, 1951 (1984).
  - [8] J.B. Suck, M. Schreiber, P. Häussler, Quasicrystals: An Introduction to Structure, Physical Properties and Applications, Springer Science & Business Media 2002.
  - [9] T. Janssen, Crystallography of quasi-crystals, Act. Crystallogr. A 42, 261 (1986).
  - [10] C. Berger, T. Grenet, P. Lindqvist, P. Lanco, J. Grieco, G. Fourcaudot and F. Cyrot-Lackmann, The new AIP-dRe icosahedral phase: Towards universal electronic behaviour for quasicrystals?, Solid State Commun. 87, 977 (1993).
  - [11] A.P. Vieira, Low-Energy Properties of Aperiodic Quantum Spin Chains, Phys.Rev.Lett. 94, 077201 (2005).
  - [12] D. Tanese, E. Gurevich, F. Baboux, T. Jacqmin, A. Lemaître, E. Galopin, I. Sagnes, A. Amo, J. Bloch and E. Akkermans, Fractal Energy Spectrum of a Polariton Gas in a Fibonacci Quasiperiodic Potential, Phys.Rev.Lett. 112, 146404 (2014).
  - [13] A. Jagannathan, The Fibonacci quasicrystal: Case study of hidden dimensions and multifractality, Rev.Mod.Phys. 93, 045001 (2021).
  - [14] C. Morfonios, P. Schmelcher, P.A. Kalozoumis and F.K. Diakonov, Local symmetry dynamics in one-dimensional aperiodic lattices: a numerical study, Nonl.Dyn. 78, 71 (2014).
  - [15] E. de Prunelé and X. Bouju, Fibonacci, Koch and Penrose structures: Spectrum of finite subsystems in three-dimensional space, Phys.Stat.Sol.(b) 225, 95 (2001).
  - [16] E. de Prunelé, Penrose structures: Gap labeling and geometry, Phys.Rev.B 66, 094202 (2002).
  - [17] M.A. Bandres, M.C. Rechtsman and M. Segev, Topological photonic quasicrystals: Fractal topological spectrum and protected transport, Phys.Rev.X 6, 011016 (2016).
  - [18] P. Vignolo, M. Bellec, J. Böhm, A. Camara, J.M. Gambaudo, U. Kuhl and F. Mortessagne, Energy landscape in a Penrose tiling, Phys.Rev.B 93, 075141 (2016).
  - [19] E. Maciá, Clustering resonance effects in the electronic energy spectrum of tridiagonal Fibonacci quasicrystals, Phys.Stat.Sol.B 254, 1700078 (2017).
  - [20] P.A. Kalozoumis, C. Morfonios, F.K. Diakonov and P. Schmelcher, Invariant of broken discrete symmetries, Phys.Rev.Lett. 113, 050403 (2014).

- [21] F.K. Diakonov and P. Schmelcher, Super-Lagrangian and variational principle for generalized continuity equations, *J.Phys. A* 52, 155203 (2019).
- [22] C. Morfonios, P.A. Kalozoumis, F.K. Diakonov and P. Schmelcher, Nonlocal discrete continuity and invariant currents in locally symmetric effective Schrödinger arrays, *Ann.Phys.* 385, 623 (2017).
- [23] P. Schmelcher, S. Krönke and F.K. Diakonov, Dynamics of local symmetry correlators for interacting many-particle systems, *J.Chem.Phys.* 146, 044116 (2017).
- [24] P.A. Kalozoumis, C. Morfonios, F.K. Diakonov and P. Schmelcher, Local symmetries in one-dimensional quantum scattering, *Phys.Rev.A* 87, 032113 (2013).
- [25] P.A. Kalozoumis, C. Morfonios, N. Palaiodimopoulos, F.K. Diakonov and P. Schmelcher, Local symmetries and perfect transmission in aperiodic photonic multilayers, *Phys.Rev.A* 88, 033857 (2013).
- [26] V.E. Zambetakis, M.K. Diakonou, P.A. Kalozoumis, F.K. Diakonov, C.V. Morfonios and P. Schmelcher, Invariant current approach to wave propagation in locally symmetric structures, *J.Phys.A* 49, 195304 (2016).
- [27] P.A. Kalozoumis, O. Richoux, F. K. Diakonov, G. Theocharis, and P. Schmelcher, Invariant currents in lossy acoustic waveguides with complete local symmetry, *Phys.Rev.B* 92, 014303 (2015).
- [28] N. Schmitt, S. Weimann, C.V. Morfonios, M. Röntgen, M. Heinrich, P. Schmelcher and A. Szameit, Observation of Local Symmetry in Photonic Systems, *Las.Phot.Rev.* 14, 1900222 (2020).
- [29] C.V. Morfonios, M. Röntgen, F.K. Diakonov and P. Schmelcher, Transfer efficiency enhancement and eigenstate properties in locally symmetric disordered finite chains, *Ann.Phys.* 418, 168163 (2020).
- [30] M. Röntgen, C.V. Morfonios, R. Wang, L. Dal Negro and P. Schmelcher, Local symmetry theory of resonator structures for the real-space control of edge states in binary aperiodic chains, *Phys.Rev. B* 99, 214201 (2019).
- [31] P. Schmelcher, Degenerate subspace localization and local symmetries, *Phys.Rev.Res.* 6, 023188 (2024).
- [32] P. Schmelcher, Isospectrally patterned lattices, *arXiv:2406.18431* (2024).
- [33] 50 Years of Anderson Localization, World Scientific, ed. by E. Abrahams (2010).
- [34] N.R. Cooper, J. Dalibard, and I.B. Spielman, Topological bands for ultracold atoms, *Rev.Mod.Phys.* 91, 015005 (2019).
- [35] Y.-T. Lin, D. M. Kennes, M. Pletyukhov, C.S. Weber, H. Schoeller, and V. Meden, Interacting Rice-Mele model: Bulk and boundaries, *Phys.Rev. B* 102, 085122 (2020).
- [36] L. Gong, W. Li, S. Zhao, and W. Cheng, A measure of localization properties of one-dimensional single electron lattice systems, *Phys. Lett. A* 380, 59 (2016).
- [37] D.C. Langreth, Sum rule for Andersons model of localized impurity states, *Phys.Rev.* 150, 516 (1966).